18.

Plasma Metamaterial Antennas and Plasma Metamaterial Frequency Selective Surfaces, Atmospheric Plasma Antennas, Plasma Resonances on Plasma Dipole Antennas, and Progress on Ruggedization of Plasma Antennas.

18.1. Plasma Metamaterials and Plasma Photonic Band Gaps for Plasma Antennas and Plasma Frequency Selective Surfaces.

A common theme in this chapter is the physics of a plasma column antenna and frequency selective surface. The author sees plasma metamaterials connected to and increasing the boundaries of plasma antennas in a similar way that metamaterial antennas are connected and expand the boundaries of metal antennas. The merging of plasma antennas and metamaterial antennas by way of plasma metamaterials could enhance the lensing of EM waves by significantly reducing the diffraction limit and enhancing cloaking by using a combination of plasma antenna and metamaterial technology. Plasma photonic band gap crystals and plasma metamaterials are much more reconfigurable than photonic band gap crystals and metamaterials and offer much larger degrees of freedom and possibilities for antenna technology.

Photonic crystals and plasma photonic crystals have been covered in various patents [1-6]. The difference between metamaterials and photonic bandgaps is essentially the wavelength. In photonic bandgaps the wavelengths are of the order of the lattice spacing, and in metamaterials the wavelengths are longer than the spacing between the lattice points. More specifically the difference between photonic crystals and metamaterials is that to have the photonic bandgap the atoms and the lattice constant in bandgaps have to be comparable in size with the wavelength, $a \approx \lambda$, because the effect of the bandgap arises from diffraction. In the case of metamaterials artificial atoms (sub-units) and lattice constant have to be much smaller than the wavelength, $a << \lambda$, because diffraction should not appear. Plasma metamaterials have a photonic-crystal-like behavior, a negative refractive index state, and a nonlinear bifurcated electric response. The wavelength passing through a metamaterial influenced by the effective parameters of the material, such as effective magnetic permeability, μ, and effective electric permittivity, ε. It is the wavelength which determines if a collection of atoms or sub-units is a material [7]. Metamaterials can have a negative refractive index. The index of refraction is given as n, where $n^2=\varepsilon\mu$. It has two components: electric permittivity, ε, and magnetic permeability, μ. A pioneer in metamaterials Veselago [8] found that there are only two available solutions for the refractive

index. When both ε and μ are positive then n>0. When both are negative then n<0. A conventional material has n>0. Materials with n<0 bend rays of incident light to the same side (as the incident beam) of the normal. Naturally-occurring materials with ε<0 include metals like silver and gold. The negative epsilon exist in the visible wavelengths. In order to obtain negative ε at longer wavelengths, a periodic structure composed of thin infinite wires arranged in a simple cubic lattice has been designed [9, 10]. In addition the magnetic response has been presented for the split-ring structure. Microwave frequencies with n<0 at is covered in [11]. Recently, negative ε and μ were demonstrated in the visible region for a material made of nanorod pairs [12,13]. Metamaterials with n<0 have applications as flat lenses. In conventional lenses with n>0 the resolution is limited by the wavelength. This is because only the far field is transmitted through a lens while the near field decays as evanescent fields. In order to increase the resolution of an image the near field has to be transmitted and amplified. This is possible with a lens made of n<0 material and has many applications [14]. By mixing a powder of BaTiO3 with nanoparticles of nickel in an appropriate ratio yields a structure with a very large dielectric constant [15]. The dielectric constant increases enormously at the percolation threshold . In the field of cloaking, it has been shown that, when an object is covered by a metamaterial made of special metal elements, the reflection (back scatter) and the shadow (forward scatter) are reduced by what is called a metamaterial cloak [16].

Fantini et al [17] published data collected for a 2D array of resonators operating in the 6–7 GHz range for separation distances of 0.25 mm and 0.5 mm in a 1–10 Torr argon gas environment. Gas breakdown data for two dielectric resonators configurations are compared to the Raizer theory at 1.1 GHz and 6.5 GHz. Plasma modulation of the reflection and transmission of dielectric resonator arrays with plasma on and off indicates possible future applications as a frequency selective surface and particularly a plasma frequency selective surface which is covered in chapter 8 of this book.

Kumar has an excellent paper on plasma photonic crystals [18]. Kumar has done very good research on plasma photonic crystals and did experiments to study the electromagnetic bands gaps (EBGs) of X-band microwave through different configurations of triangle structure of MPC with and without plasma columns, and measured transmitted power of 18 GHz with electrodes (without plasma between electrodes) and with plasma between the electrodes. Kumar further showed by switching ON and OFF the plasma column, propagation of microwave in metallic photonic crystal can be controlled in such a way that positive and negative refraction can be achieved and concluded from the fact that plasma can be used to form tunable / controllable photonic crystals.

A fully tunable plasma photonic crystal and plasma metamaterials can be used to control the propagation of free space electromagnetic waves and can be used in antenna technology. Light propagation in photonic crystals is the result of Bragg diffraction for each atom which is a result of the periodic structure of the photonic crystals.. Light waves in photonic crystals can be modeled as Bloch waves. An effective

index of refraction including a negative index of refraction for the crystal is used to describe the overall reflectivity form the photonic crystal.

A plasma photonic crystal can be an array of discharge plasma tubes which form a lattice structure with the individual plasma dielectric constant tuned through variation in the plasma density. Plasma photonic crystals can be used to tune and control microwave propagation. A schematic of a plasma photonic bandgap crystal can be found in [18] which if the wavelengths of the EM waves are longer than the distances between the lattice points becomes a plasma metamaterial. Plasma photonic band gap crystals and plasma metamaterials are much more reconfigurable than photonic band gap crystals and metamaterials and offer much larger degrees of freedom and possibilities for antenna technology.

Plasma metamaterial pass wavelengths longer than the lattice spacing in a plasma photonic bandgap. In the same way, metamaterials are used in antennas to form metamaterial antennas, plasma metamaterials can be used to form plasma metamaterial antennas.

Kumar [18] developed a schematic of a hybrid plasma photonic crystal if the wavelengths of the electromagnetic waves are on the order of the spacing between the lattice points. If the wavelengths of the EM waves are longer than the distances between the lattice points this is a schematic of a plasma hybrid metameterial.

Figure 18.1 [19] is schematics for EM waves passing through plasma bulk, plasma photonic bandgaps and plasma metamaterials, hybrid plasma photonic bandgap crystals and hybrid plasma metamaterials, and plasma photonic bandgaps and plasma metamaterials with plasma resonators.

Plasma photonic bandgap crystal through simulations and experiments have shown that transverse electric mode bandgaps exist, arising from the positive and negative dielectric constant regimes of the plasma Wang et al [20]. This showed that the respective bandgap frequencies shifted through changing the dielectric constant by varying discharge current density.

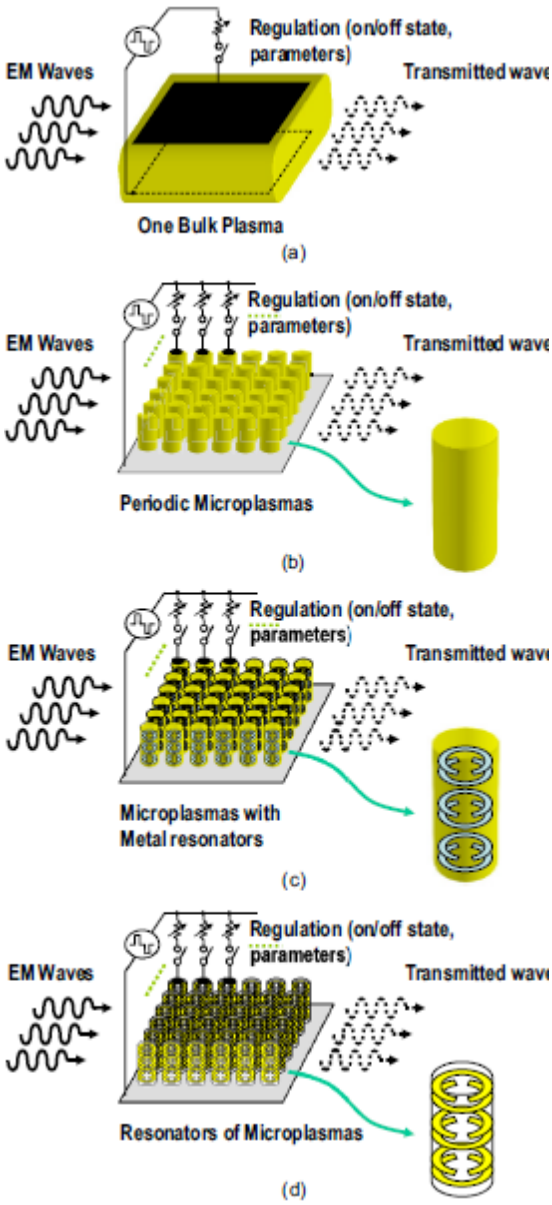

Figure 18.1. (a).A schematic of EM waves passing through a bulk plasma. (b). A schematic of EM waves passing through a plasma photonic bandgap crystal which If the wavelengths of the EM waves are longer than the distances between the lattice points becomes a plasma metamaterial. (c). A schematic of EM waves passing a hybrid plasma photonic crystal if the wavelengths of the electromagnetic waves are on the order of the spacing between the lattice points. If the wavelengths of the EM waves are longer than the distances between the lattice points this is a schematic of a plasma hybrid metamaterial. (d).). A schematic of EM waves passing through a plasma photonic bandgap crystal with micro-plasma resonators which If the wavelengths of the EM waves are longer than the distances between the lattice points becomes a plasma metamaterial.

Tan et al [21] by using finite-element methods, did research on the effect of plasma density on the photonic bandgap of 1-D plasma photonic crystals.. Below the cutoff frequency, the transverse electric (TE) mode bandgaps exist due to the surface modes such as the bandgaps in metallic photonic crystals. Above the cutoff frequency the positive permittivity bandgaps for TE mode such as the bandgaps in conventional photonic crystals are a consequence of the periodic distribution of dielectric constant in plasma and background medium. The bandgaps of the all plasma photonic crystals are strongly dependent on the plasma density.

18.2 Experiment in Scattering Electromagnetic Waves off of Metal Photonic Crystal with a Metal Tube Replaced by a Plasma Column.

Scattering electromagnetic waves off of a photonic metal crystal is fixed and it can only be reconfigured if the metal tubes are mechanically removed or altered. With plasma tubes the hybrid or pure plasma photonic crystal is reconfigurable by extinguishing the plasma or creating the plasma tubes.

In this experiment one tube of an array of metal tubes comprising a metal photonic crystal is replaced by a plasma tube and the plasma tube is turned off (plasma extinguished) or plasma created and the scattering of electromagnetic waves is reconfigured. This is a first step toward demonstrating the reconfiguration of hybrid photonic band gaps by turning a plasma tubes or tubes off and on and scattering electromagnetic waves off of both reconfigurations. These results can be extended to plasma metamaterials by increasing the wavelength compared to the lattice constant so that the distance between lattice sites is small compared to a wavelength.

In this experiment by Kumar [18] 18 GHz is scattered through the hybrid photonic band gap. The plasma tube is turned on and off and the results are observed. The plasma density is 5x10^12cm^-3. The electron temperature is 2 eV at atmospheric pressure. There are 33 copper tubes and one plasma tube with diameters 2 mm and length of 100 mm. The lattice constant of 10 mm. The electromagnetic waves which scatter off of the hybrid photonic band gap crystal are from 2 GHz to 28 GHz. The cathode voltage is 800 V and anode voltage is 1 KV to 2 KV with a current of 15 mA. The transmitted power is -38 dBm at 45 degrees incident angle with the plasma off and -48 dBm with the plasma on.

In addition Kumar [18] did an experiment with an array in a triangular lattice as shown in the schematic in [18].with 33 copper tubes an electrode pair which turns a plasma off and on. This is a hybrid photonic bandgap. Kumar shows the scattering angle where the transmitting antenna is a horn antenna and the receiving antenna is also a horn antenna. Kumar shows the scattering with the plasma off and the scattering with the plasma on.

Kumar showed the results of the experiment with the transmitted power plotted against the scattering angle with the plasma extinguished with just electrodes and with the plasma on.

18.3 Atmospheric Plasma Antennas

Atmospheric plasma antennas can be formed by ionizing paths in the atmosphere and discharging along those paths with a Marx Generator. Several atmospheric plasma antenna designs are in a publicly released Navy document by Anderson [22]. In this case the application of an atmospheric plasma antenna was an ELF antenna because it seems like the only way to create an ELF antenna was with a long atmospheric plasma antenna. A metal antenna of that length would be very long and heavy. Patents [23, 24] have been issued on atmospheric plasma antennas. Dwyer et al [25] built and did measurements on an atmospheric discharge plasma antenna. They created the plasma by a laser-guided, electric discharge in the atmosphere and shaped it into a folded monopole plasma antenna. This atmospheric discharge plasma antenna has been used to transmit and receive signals at 112 MHz [26]. A comparison was made with a folded copper antenna of the same size. The signal transmitted and received on the plasma antenna was 2 dB or less of the corresponding copper antenna. In their experiments the noise from the plasma antenna was indistinguishable from the noise from the copper antenna. Figure 18.2 [25] is a schematic for the design of the atmospheric discharge plasma antenna. Figure 18.3 [25] is a schematic for the design the high voltage system used to create the atmospheric discharge plasma antenna. Table 18.1 shows the results of the experiments.

Transmitting antenna**	Receiving antenna	Transmitting VSWR	Received Signal dB*
Copper	Copper	2.78	0
Copper	Plasma	2.78	+1
Plasma	Copper	3.45 to2.04	-2

*Measured with respect to the copper/copper antenna system.

**Incident power on antennas is 0.25 watts at 112 MHz.

Table 18.1. Results of measurements of the atmospheric discharge antenna.

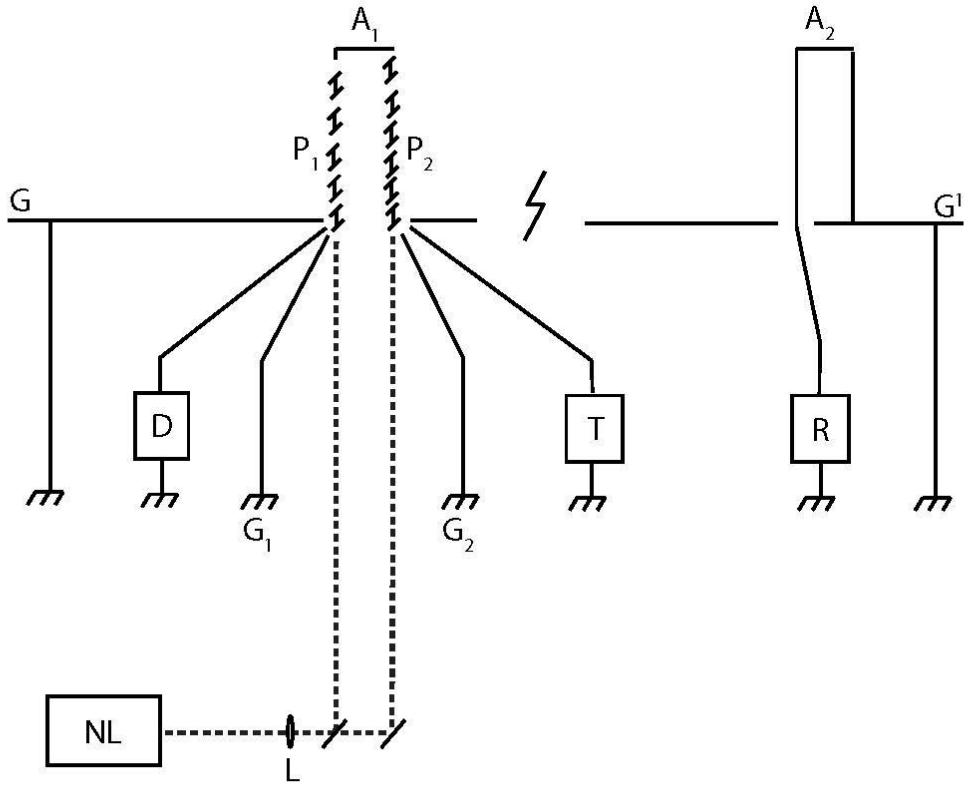

Figure 18.2. Schematic of the atmospheric plasma antenna experiment.

A_1 is the top part of the plasma antenna. P_1 and P_2 are the vertical paths of the plasma antenna . G is the ground plane for the plasma antenna. A_2 is the top part of the copper antenna. G^1 is the ground plane for the copper antenna. NL represents the Nd: glass laser. L is the focal length lens. D is the high voltage system that drives the high voltage system and goes to the ground G_2. T is the RF transmitter and G_1 is the RF ground. R is the receiver.

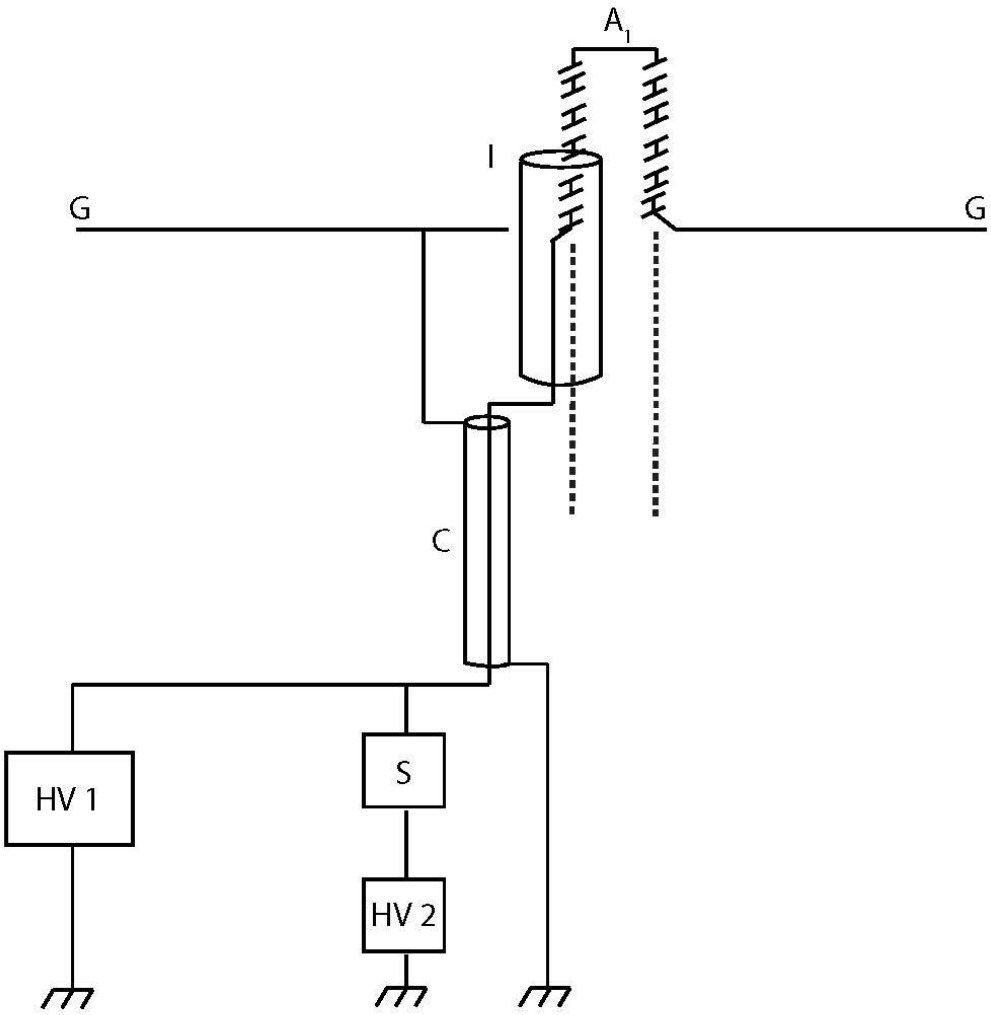

Figure 18.3. Schematic of the high voltage system used to create the plasma antenna. HV1 is the Marx generator. HV1 is less than or equal to 360kV. HV2 is the capacitor bank. HV2 is less than or equal to 20 kV. S is the activated solid dielectric closing switch. C is the high voltage coaxial line. G is the ground plane for the plasma antenna. A_1 is the top part of the plasma antenna. I is an insulator plastic tube.

18.4 Plasma Resonances on a Cylindrical Plasma.

18.4.1 Experiments and simulations on plasma resonances of a cylindrical plasma column.

See section 2.4 for scattering of electromagnetic waves from a plasma cylinder. Resonances were observed by Tonks [27] in scattering electromagnetic waves off of a cylindrical column of plasma. Experiments on scattering off of cylindrical plasmas can give valuable information on the utility of plasma antennas and plasma FSS. Tonks studied plasma discharge cylindrical columns and performed experiments of scattering electromagnetic waves off of a plasma cylindrical column. A schematic of the basic physical interaction is given in Figure 18.4. The experimental setup of the Tonks experiment is given in Figure 18.5. An electromagnetic wave from a signal source is propagated into a waveguide with dimensions corresponding to a cutoff wavelength of 10 cm. A thermionic-arc discharge column is situated at right angles to the incident waveguide electric field. Two direction couplers sample the amplitude of the incident wave and the amplitude of the reflected wave. The experiment consists of measuring the ratio of the scattered power reflected by the plasma to the power incident on the plasma as a function of the density of the plasma. The discharge column is a thermionic-arc discharge in mercury vapor at a pressure (10^-3 Torr) such that the plasma electron density is proportional to the dc current in the discharge. The plasma is collisionless since the mean free path of plasma electrons is much greater than the diameter of the plasma columns. The wavelength of the incident wave is much greater than the radius of the plasma column so that the electric field in the vicinity of the plasma column is nearly irrotational and the electric field can be derived from a scalar potential. The electrical potential satisfies Laplace's equation with no z variation, both inside and outside the plasma. The boundary conditions at a dielectric-vacuum interface are that the normal component of the displacement and tangential component of the electric field be continuous. These conditions are satisfied at the plasma-air boundary.

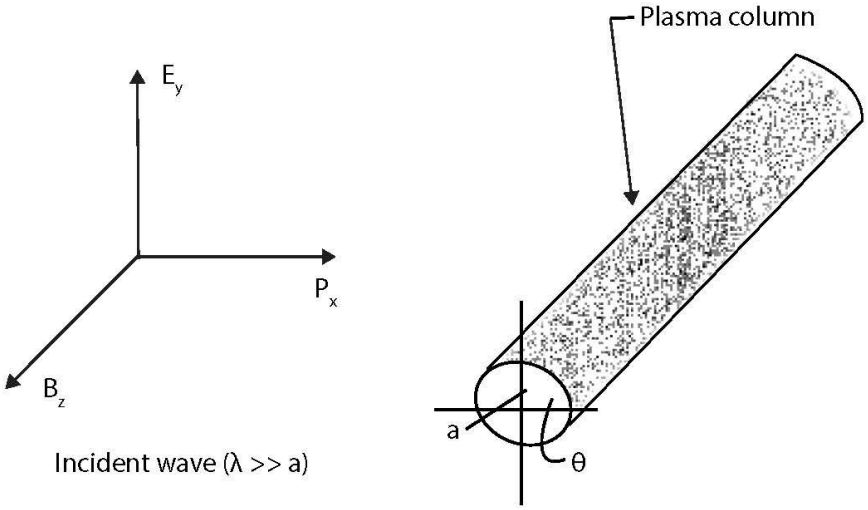

Figure 18.4. Scattering experiment basics showing incident polarization of the EM waves and the target plasma column.

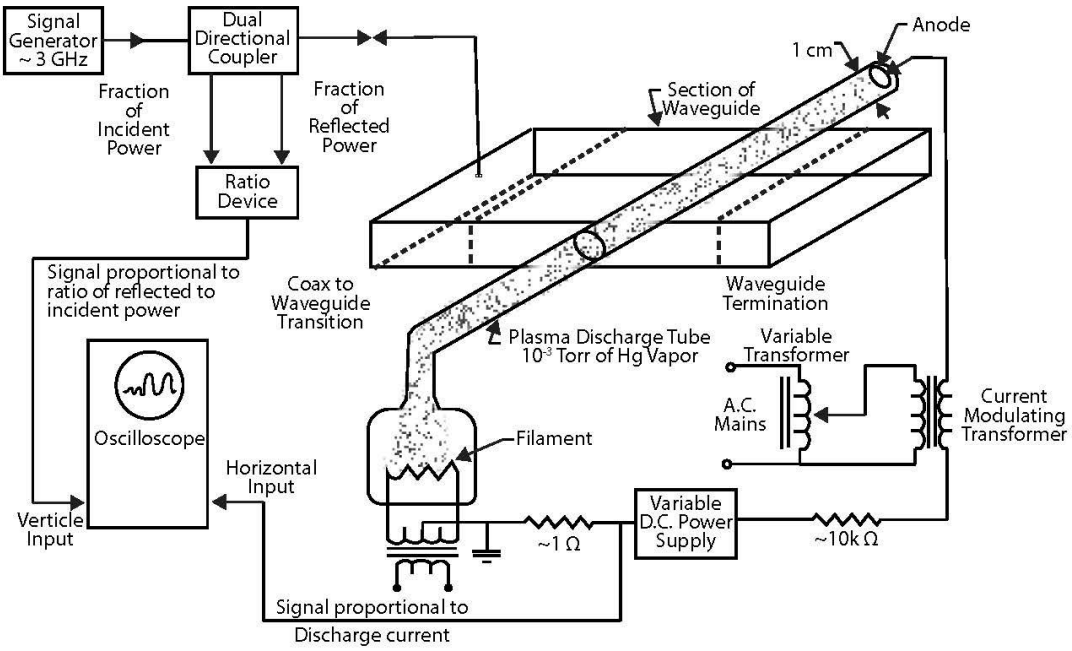

Figure 18.5. Experimental set up of the Tonk's scattering experiment of electromagnetic waves off of a plasma cylindrical column.

The results of the Tonk's scattering experiment are given in Figure 18.6

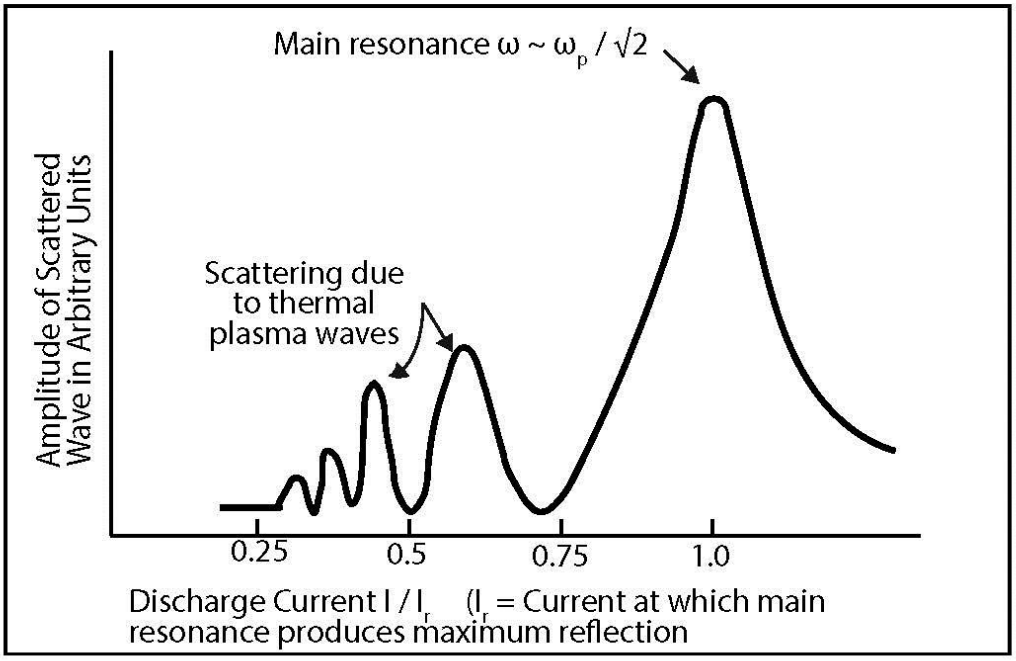

Figure 18.6. Amplitude of Scattered waves as a function of discharge current or plasma density. The peak resonance occurs at the plasma frequency divided by the square root of two. The square root of two factor comes in on the cylindrical geometry.

18.4.2 Simulations and experiments of resonances in a plasma dipole antenna with a 100 MHz to 5 GHz sweep.

The plasma dipole antenna has a length of 7.5 cm and a diameter of .25 cm. There are two capacitive bands connecting the feeds to the plasma dipole antenna in the center. In a simulation, a frequency sweep was done on the plasma dipole antenna from 100 MHz to 5 GHz. The plasma has a density of 10^19m^-3. The resonances in the radiated power [private communication with D. Melazzi, 2015] are given are given in Figure 18.7 as well as a comparison to the same dipole antenna as a perfectly electric conductor (PEC). The resonance in the impedance is shown in Figures 18.8 and 18.9 [28]. An experiment was done by scattering electromagnetic waves off of a cylindrical plasma and sweeping from 100 MHz to 5 GHz. The results shown in Figure 18.16 shows the results of this scattering experiment with major and minor resonances similar in form to the simulation of Figure 18.12.

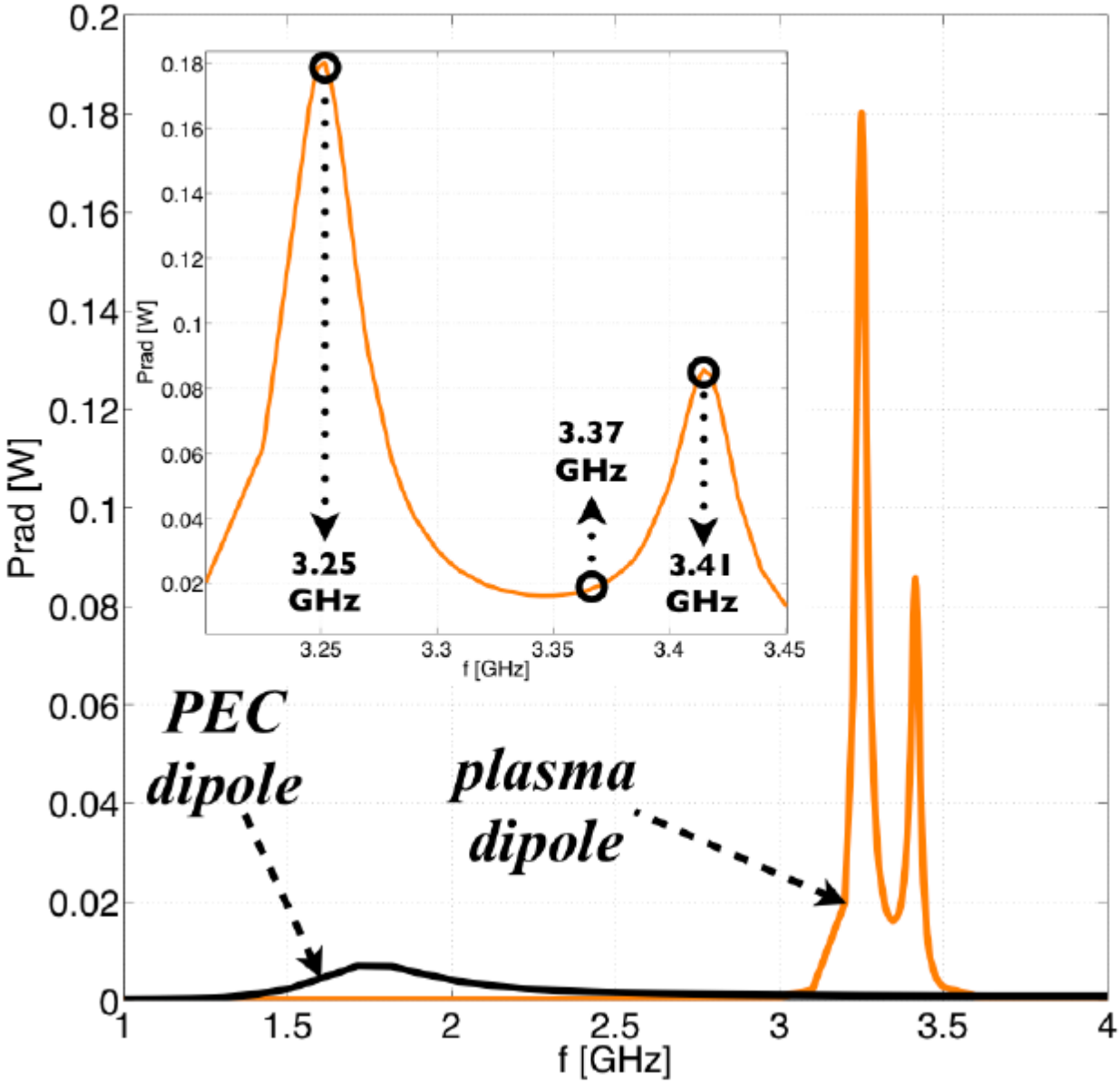

Figure 18.7. Simulation with frequency sweep from 100 MHz to 5 GHz on the plasma dipole antenna with density 10^19^m-3.showing the radiated power. The background pressure of the plasma was 15mT and the electron temperature is 3 eV. This also shows the result of the PEC (perfect electrical conductor) dipole of the same length. [private communication with Davide Melazzi]

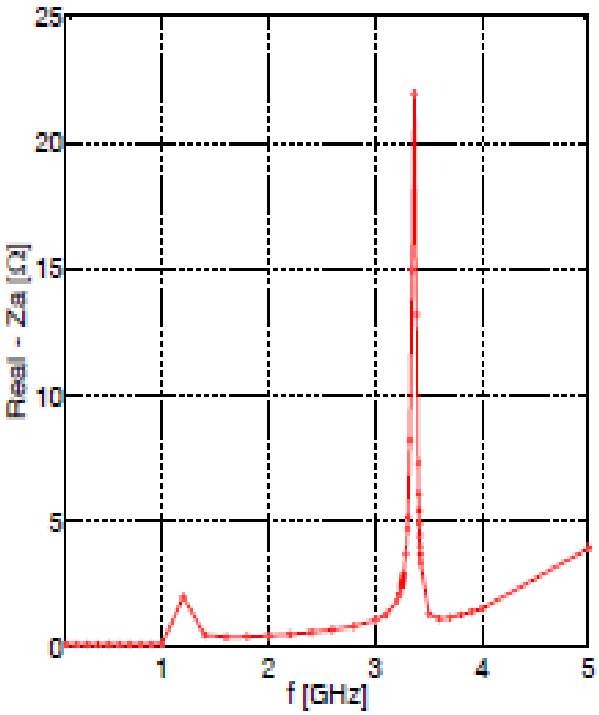

Figure 18.8. This shows the real apert of the impedance resonantes between 3 GHz and 3.5 GHz. The real part of the impedance is 22 Ohms. Frequency sweep was from 100 MHz to 5 GHz on the plasma dipole antenna with density 10^19^m-3.showing resonances in the imaginary part of the impedance. The background pressure of the plasma was 15mT and the electron temperature is 3 eV. [private communication with Davide Melazzi] [28].

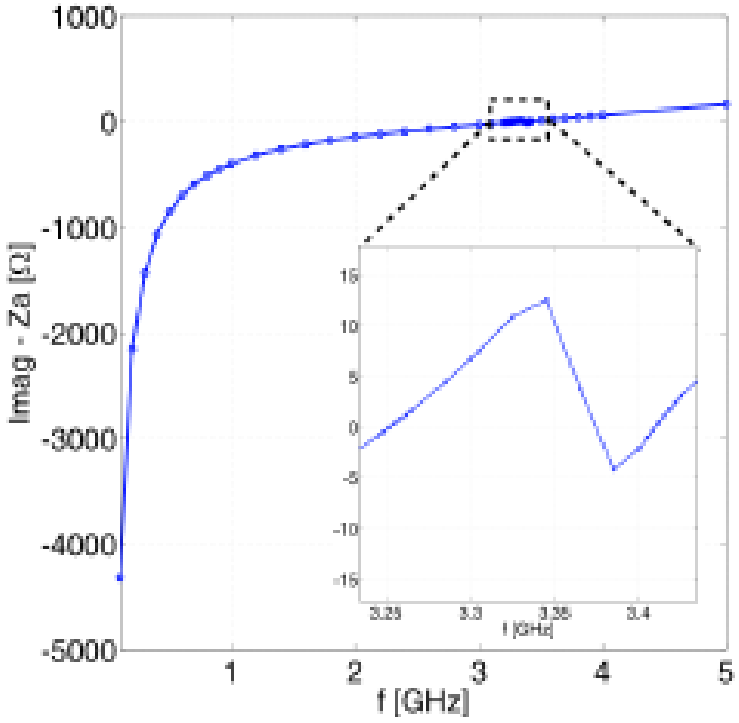

Figure 18.9. is a plot of the imaginary part of the impedance and corresponds to the real part of the impedance Figure 18.8. [private communication with Davide Melazzi] [28]

An experiment was done to observe resonances in the scattering of electromanetic waves off of a plasma cylinder as shown in Figure 18.10. A basic pulsing mechaism was used to ionize the plasma.The frequency sweep was given between 100 MHz and 5 GHz. The results are given in Figure 18.11. Major and minor resonances were observed as was predicted by the simulation in Figure 18.7.

Figure 18.10. Experimental setup for scattering electromagnetic waves off of a plasma dipole antenna and sweeping from 100 MHz to 5 GHz. This is an early experiment with early pulsing device.

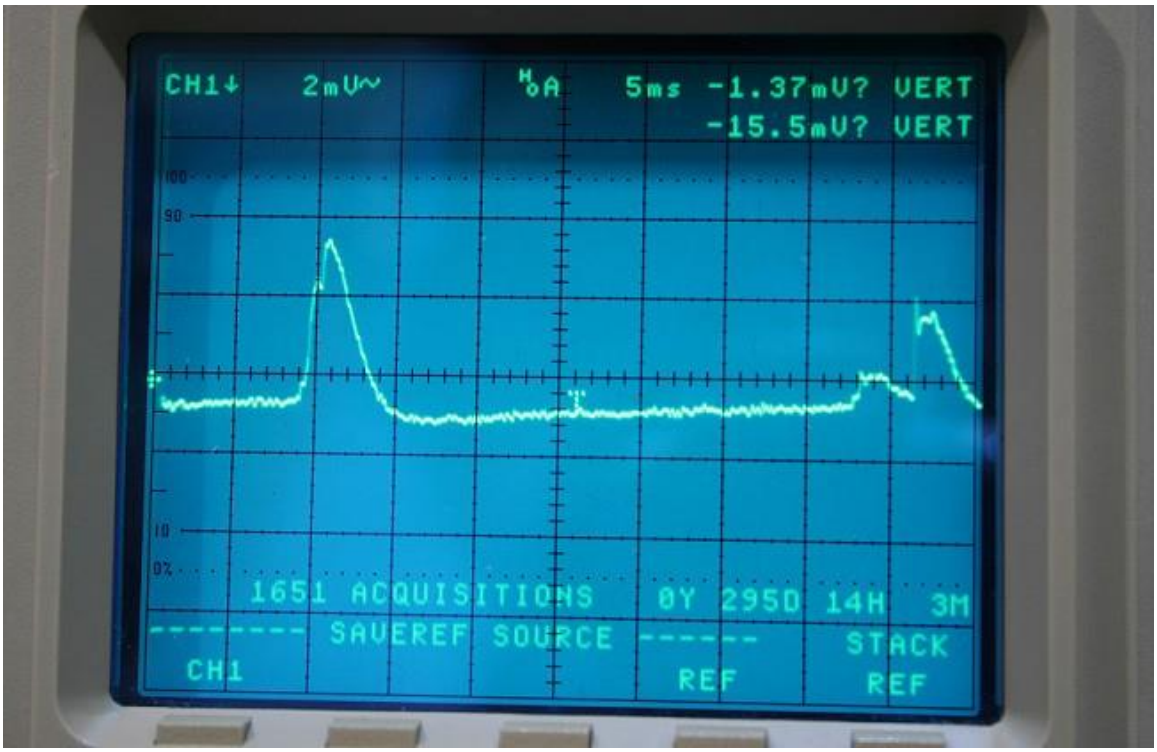

Figure 18.11. Results of the scattering experiment of Figure 18.10. Major and minor resonances are observed as is shown in the simulation of Figure 18.7.

18.4.3 Understanding some charateristics of the plasma by pulsing the plasma and observing the plasma recombination or decay of a cylindrical plasma column.

To understand the plasma resonances better with possible very positive advantages to plasma antennas, the plasma was pulsed and the plasma allowed to decay to observe any resonate effects as the plasma frequency changed through a variety of frequencies compared to the operating frequency. While the plasma was pulsed in a COTS (commercial off the shelf) tube a Klystron oscillator transmitted electromagnetic waves at 10 GHz through the plasma tube into a receiving horn antenna. Polarization is perpendicular to the axis of the tube . The Klystron oscillator is shown in Figure 18.12. The Klystron is in the foreground and an X-band horn with crystal detector is shown on the opposite side of the plasma tube. For 24 GHz a Gunn diode transmitter was used instead of a Klystron at 10 GHz. The plot of the received transmission signal with ionization of the gas in the plasma tube by a 10 Amp peak ionization current and subsequent recombination and decay of the plasma was observed. There were voltage spikes in the measurements.. The received signal showed received signal transmission vs. time with a 20 A peak ionization current. A sharp downward transition indicated current pulse and maximum plasma density. The disturbance in the smooth waveform during plasma density decays but shows some disturbances. A remarkable observation was the second horizontal line from the bottom horizontal line. This line was the received transmission signal at 24 GHz Gunn diode with the plasma in the tube extinguished. The received signal during the pulse and subsequent

decay of the plasma is both above and below this line indicating an amplification for the received signal above the line for the received signal with no plasma. The transmission of a 24 GHz Gunn diode through a plasma was formed by pulsing with 10 Amp peak current and the plasma was allowed to recombine or decay for observation. There were spikes in the measurements. The scales for the test results were 10 milli-Volt per division for vertical axis and 250 microseconds per div. on horizontal axis.

Figure 18.12. Experimental setup for observation of plasma characteristics in the plasma recombination or plasma decay. The Klyston transmits in the X band at 10 GHz. The plasma is pulsed and allowed to recombine or decay and observations are made. Polarization is

perpendicular to the axis of the tube. Klystron oscillator is shown in the foreground and an X-band horn with crystal detector is shown on the opposite side of the plasma tube.

18.4.4. Simulations on a plasma dipole antenna as a function of density and gas type.

In section 15.10 results of simulations on plasma dipoles were given. Continuing with the characteristics of a plasma dipole antenna, we show the results of simulations of the radiation patterns as function of plasma density Figure 18.13 [28] and plasma gas type Figure 18.14 [28]. In both cases, the background pressure of the plasma was 15mT and the electron temperature is 3 eV.

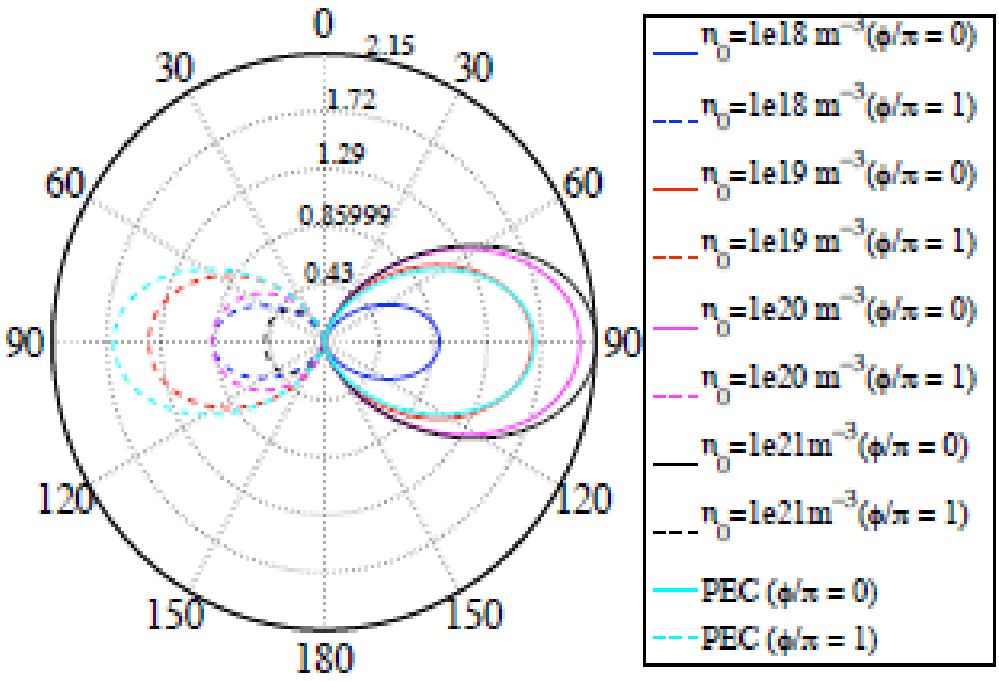

Figure 1813.[28] Radiation patterns for the same plasma dipole antenna as a function of plasma density and a PEC (perfect electrical conductor). The background pressure of the plasma was 15mT and the electron temperature is 3 eV. This plasma dipole with its size, gas pressure, and temperature has a maximum directivity at a plasma density of 1e21m^{-3}.

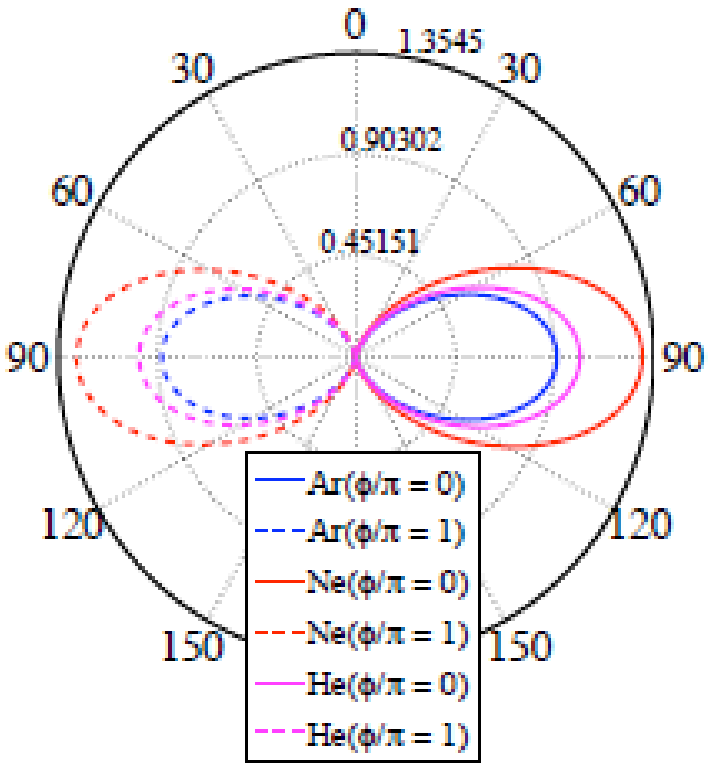

Figure 18.14. Radiation patterns for the same plasma dipole antenna as a function of the type of gas with Ar for Argon, Ne for Neon, and He for Helium. The background pressure of the plasma was 15mT and the electron temperature is 3 eV. In this plot under these conditions of this pressure, temperature, and geometry, Neon gives the highest directivity. Argon however is less expensive.[28]

18.4.5. Electrically Small Monopole Antennas using Plasma Physics

Vincent Laquerbe and Romain Pascaud et al [29] have developed an innovative way to build antennas that are electrically small using plasma physics. It has been suggested in [30] and [31] that electrically small antennas could be made with plasma physics. The Vincent Laquerbe and Romain Pascaud team[29] were able to create a $\lambda/9$ monopole antenna as an equivalent to a $\lambda/4$ monopole antenna. The S11 for the electrically small antenna was very close to the S11 $\lambda/4$. However the S12 for the electrically small antenna placed in the hemispheric plasma envelop was 8 dB less than the S12 of the $\lambda/4$ monopole at the resonance frequency of 310 MHz. The hemispherical dome was filled with a mixed gas of 99% Neon and 1 % Xenon and was ionized The gas was ionized into a plasma by an RF spiral coil. The antenna was inside the dome and surrounded by plasma of 10 mT. The hemispherical dome was configured such that the relative permittivity is equal to -2. Under these conditions, a localized surface plasmon resonance was formed. When the plasma frequency is greater than the operating frequency, the collision frequency is much less than the operating frequency, and when the relative permittivity is equal to -2, the operating frequency will equal to the plasma frequency divided by the square root of 3. This is the same result that is obtained for the resonant peak in scattered waves from a sphere in section 18.1.3. For scattering of electromagnetic waves off of a cylinder the resonant peak occurs when the operating frequency equals the plasma frequency divided by the square root of 2 as Figure 18.6 shows.

18.5. Minimum Ionization Current to Create a Plasma Antenna

The Figure shows the received signal at 1.25 MHz as a function of DC plasma discharge current. [private communication with Fred Dyer] The signal is coming from a local AM radio station operating at 1250 KHz. Received signal strength is measured by a B&K Precision spectrum analyzer. Signal strength at the input of the spectrum analyzer is on the order of -80 dBm. The signal is displayed normalized in the above plot in order to easier visualize relative signal strengths. Received signal strength is unchanged for currents greater than 4 mA. At lower currents the signal strength quickly decreases. A signal can be received at 1 mA DC plasma discharge current or less as Figure 18.15.

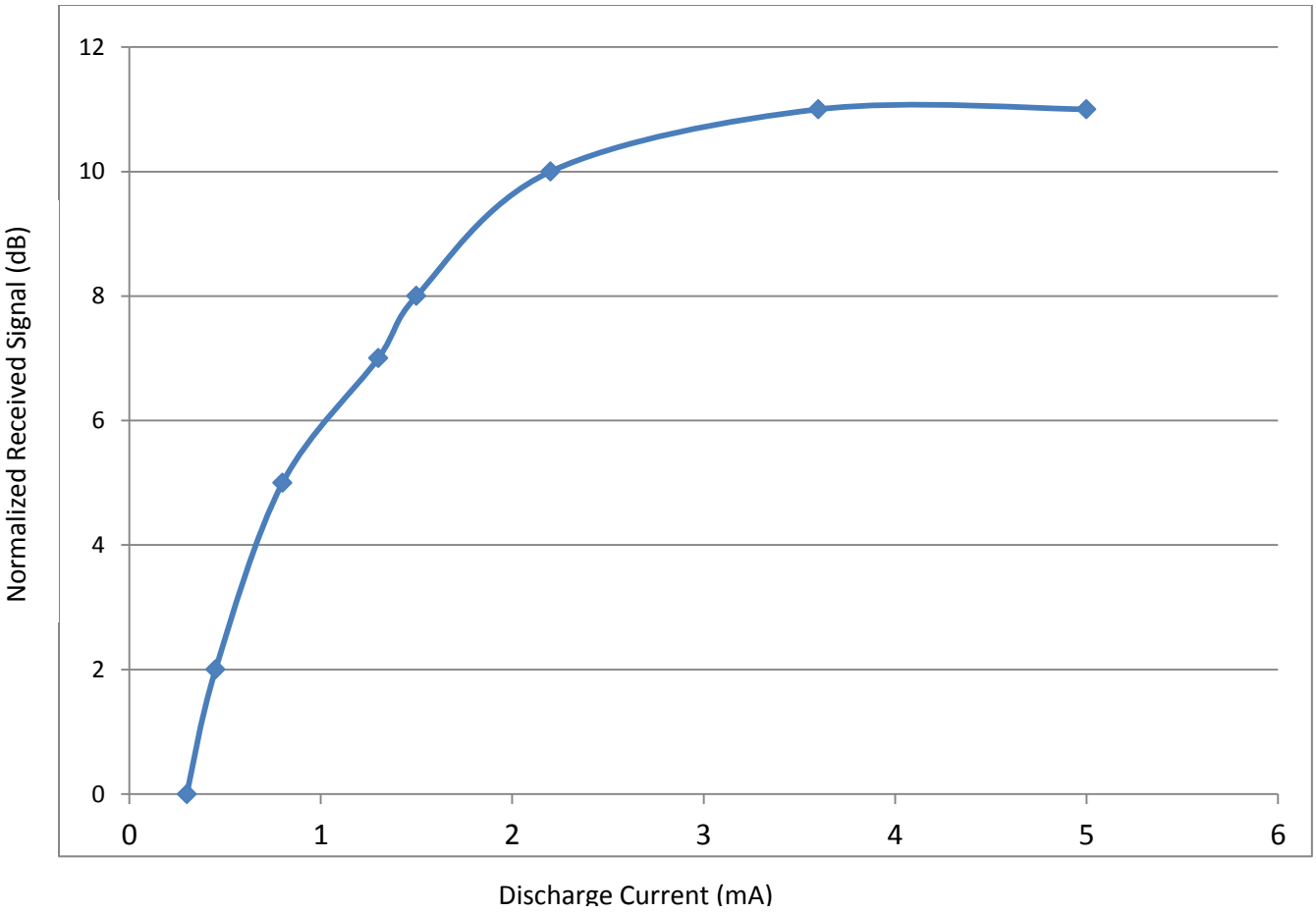

Figure 18.15 Received signal from plasma antenna vs. plasma discharge current. Frequency is 1.25 MHz, a local AM radio station. [private communication with Fred Dyer, 2020].

18.6 Pre-ionization Current to Make Ionization faster and with Less Power

Pre-ionization using a very small bias current flowing [private communication with L.Barnett, 2020], e.g. 1 uA DC in an "off tube" will significantly reduce the energy to start and maintain the plasma.

Very low level radioactive seeds can be put into custom made plasma tubes to give enough pre-ionization. Significantly reduce the energy to start and maintain the plasma. Given issues with radioactive seeds, the small bias method is better.

18.7. Progress on Ruggedization on Plasma Antennas.

Ruggedization of plasma antennas is covered in section 9.12 in this book. Since then SynFoam [32] used to ruggedize plasma antennas is much more advanced. It is light in weight, has an index of refraction close to one, and very rugged.

A 1-dimensional plasma focusing system for Ku band (12-14 GHz) is being ruggedized [Private communication with L. Barnett, 2019]. An array of tubes spaced close enough together appear as a near continuous plasma. Borosilicate glass will be used as it is relatively easy to work with and durable, but fused quartz is another option. Tougher glasses like Gorilla Glass [33] and Diamond Glass or even ceramics with hard sealed brazing are being used. Rugged Kovar end caps are being assembled (with OFHC copper tubulations and tungsten wire electrodes) with a high temperature epoxy (343 C max working temperature) used by NASA on spacecraft, rather than glassblowing, as being a simpler, faster, and cheaper option.

The plasma/metal reflector would have a plate or array of plasma tubes attached to a flat metal plate which provides higher ruggedization and conduction cooling. For even higher ruggedization, the front surface of the ceramic plate with Lexan glass could be very thick and also overcoated with soft, radome dielectric material, of several or (even many) cm thickness, and provide very high resistance to bullets, shrapnel, and high pressure shock waves (as from nearby explosions) that would easily disable a conventional antenna. Rather than being fragile, the array of tubes or plate containing plasma alone, or coupled with flat metal plate reflector design, could be more survivable than any fast tracking metal phased array type.

Research is being done to ruggedize plasma antennas by embedding Gorilla or Diamond glass tubes in hardened syntactic form called SynFoam or ruggedized ceramics. Other approaches are using Teflon tubing and Ultra-High Molecular Weight (UHMW) polyethylene tubing to test for possible use as a plasma tube. Both types of tubing have flexibility, non-conductivity, and high temperature resistant. The device for creating a vacuum in the tube and back filling with Argon, Neon, Helium, or Xenon gas was used.

Going forward with research on the ruggedization of plasma antennas, the miniaturization and ruggedization of glass tubes made with gorilla glass embedded in SynFoam or rugged ceramics is very promising.

18.8. Radio Communication with Hypersonic Aerial Vehicle by Treating Plasma Sheath as an Antenna.

The plasma sheath formed around a hypersonic craft [34-38] has a plasma frequency above communications frequency and are reflected and/or heavily attenuated. By using the plasma sheath as a plasma antenna and coupled to the craft with a surface wave launcher or surfatron the plasma sheath can be coupled to and forming a plasma antenna.

References

[1]. T. Anderson, *Configurable arrays for steerable antennas and wireless network incorporating the steerable antennas*. Patent No. 6,870,517, March 11, 2008.

[2]. T. Anderson, *Configurable arrays for steerable antennas and wireless network incorporating the steerable antennas*. Patent No. 7,342,549, March 22, 2005

[3. T. Anderson, *Reconfigurable scanner and RFID system using the scanner*, Patent No. 6,922,173, July 26, 2005

[4]. T. Anderson, *Tunable plasma frequency devices*, Patent No. 7,292,191.November 6, 2007

[5]. T. Anderson, *Tunable plasma frequency devices*, Patent No. 7,453,403. November 18, 2008

[6]. T. Anderson, *Reconfigurable scanner and RFID*. Patent number RE43, 699. July 18, 2007

[7]. SMITH, D. R., PENDRY, J. B., WILTSHIRE, M. C. K., *Metamaterials and negative refractive index.* Science, 305: 788 (2004).

[8]. VESELAGO, V. G., *The electrodynamics of substances with simultaneously negative values of ε and μ,* Sov. Phys. Usp. 10: 509 (1968).

[9]. PENDRY, J. B. et al., *Extremely low frequency plasmons in metallic mesostructures,* Phys. Rev. Lett., 76: 4773 (1996).

[10]. PENDRY, J. B., *Low Frequency Plasmons in Thin Wire Structures,* J. Phys. Cond. Matt.10; 4785 (1998).

[11]. SHELBY, R., SMITH, D. R., SCHULTZ, S., *Experimental verification of a negative index of refraction.* Science, 292: 77 (2001).

[12]. SHALAEV, V. M. et al., *Negative index of refraction in optical metamaterials*. Opt. Lett.30; 3356 (2005).

[13] LAGARKOV, A. N., SARYCHEV, A. K., Electromagnetic properties of composites containing elongated conducting inclusions. Phys. Rev. B 53: 6318 (1996).

[14]. PENDRY, J. B., SMITH, D. R., *Reversing light: negative refraction*, Physics Today, December 2003.

[15]. PECHARROMAN, C., ESTEBAN_BETEGON, F., New percolative BaTiO3-Ni composites with a high and frequency-independent dielectric constant (εr=80 000). Adv. Mater., 13: 1541 (2001).

[16]. SCHURIG, D., MOCK, J.J., JUSTICE, B.J., CUMMER, S.A., PENDRY, J.B., STARR, A.F., SMITH, D.R. , Metamaterial electromagnetic cloak at microwave frequencies, Science, 314: 403 (2006).

[17] Lisa Fantini, Stephen Dennison, Hyunjun Kim, Maryam Sarkarat, Michael Lanagan and

Jeffrey Hopwood; *Plasma reconfigurable metamaterial using a 6.5 GHz dielectric resonator array;* Journal of Applied Physics 126, 203301 (2019); https://doi.org/10.1063/1.5121222.

[18]. Rajneesh Kumar, *Plasma Photonic Crystal*, 2012 InTech Open, Chapter 14.

[19]. Osamu Sakai and Kunihide Tachibana, *Plasmas as metamaterials: a review*, Received 10 June 2011, in final form 4 November 2011 Published 31 January 201 Online at stacks.iop.org/PSST/21/013001, IOP PUBLISHING PLASMA SOURCES SCIENCE AND TECHNOLOGY, Plasma Sources Sci. Technol. 21 (2012) 013001 (18pp)

[20]. B. Wang and M. A. Cappelli, *A plasma photonic crystal bandgap device*, Appl. Phys. Lett. 108, 161101 (2016); https://doi.org/10.1063/1.4946805

[21]. Haiyun Tan ; Chenggang Jin ; Lanjian Zhuge ; Xuemei Wu, *Simulation on the Photonic Bandgap of 1-D Plasma Photonic Crystals,* Journal of Applied Physics 126, 203301 (2019);

[22]. Anderson, T, *ELF PLASMA ANTENNA*, NUWC-NPT Technical Memorandum 972159, https://apps.dtic.mil/dtic/tr/fulltext/u2/a637098.pdf, 30 September 1997.

[23]. Anderson, T., *Laser driven plasma antenna utilizing laser modified Maxwellian Relaxation.* Patent number 6,650,297, November 18, 2003.

[24]. Anderson, T., Plasma antenna with electro-optical modulator. Patent number 6,087,993, July 11, 2000.

[25]. TLMOTHY J. DWYER. JOSEPH R. GREIG, DONALD P. MURPHY, JEFFREY M. PERIN, ROBERT E. PECHACEK, *On the Feasibility of Using an Atmospheric Discharge Plasma as an RF Antenna,* IEEE Transactions on Antennas and Propagation (Volume: 32 , Issue: 2 , February 1984), Page(s): 141 – 146.

[26] J. R. Greig. R. F. Femsler. D. P. Murphy, R. E. Pechacek. J . M. Perin. and M. Raleigh. "Laser-guided electric discharges in the atmosphere." in Proc. 7th Int. Conf. Gas Discharges and their Appli. London, Aug. 1982. p. 464.

[27] Tonks, L., "The High Frequency Behavior of a Plasma," Phys. Rev. Vol. 37, 1931, p.1458

[28]. Davide Melazzi, Paola De Carloy, Vito Lancellottiz, Fabio Trezzolaniy, Marco Manentex and Daniele Pavarin, *Radiation Properties of a Gaseous Plasma Antenna*, EuCAP 2016.

[29]. Vincent Laquerbe, Romain Pascaud, Thierry Callegari, Laurent Liard, Olivier Pascal; *Towards Antenna Miniaturization Using Plasma;* 13th European Conference on Antennas and Propagation (EuCAP 2019).

[30] H. R. Stuart and A. Pidwerbetsky, “Electrically small antenna elements using negative permittivity resonators,” IEEE Trans. Antennas Propag.,vol. 54, no. 6, pp. 1644–1653, Jun. 2006.

[31] R. Ziolkowski and A. Erentok, “Metamaterial-based efficient electrically small antennas,” IEEE Trans. Antennas Propag., vol. 54, no. 7, pp. 2113–2130, Jul. 2006.

[32]. https://synfoam.com/

[33]. https://www.corning.com/gorillaglass/worldwide/en.html

[34]. Chadwick, K.M., Boyer, D.W. and Andre, S.S. “Plasma and Flowfield Induced Effects on Hypervelocity Reentry Vehicles for L-Band Irradiation at Near Broadside Aspect Angles.” 27th AIAA Plasmadynamics and Lasers Conference, New Orleans, LA, June 1996. https://arc.aiaa.org/doi/10.2514/6.1996-2322

[36].Norris, G. “Plasma Puzzle: Radio Frequency-Blocking Sheath Presents a Hurdle to Hypersonic Flight.” Aviation Week & Space Technology, March 2009, p. 58.

[37]. Blottner, F.G. “Viscous Shock Layer at the Stagnation Point with Nonequilibrium Air Chemistry.” AIAA Journal, vol. 7, no. 12, December 1969, pp. 2281-2288. https://arc.aiaa.org/doi/abs/10.2514/3.5528?journalCode=aiaaj

[38]. Hartunian, R.A. et al. “Implication and Mitigation of Radio Frequency Blackout during Reentry of Reusable Launch Vehicles.” AIAA Atmospheric Flight Mechanics Conference, Hilton Head, South Carolina, Aug 20-23, 2007